Materials Research Proceedings **21** (2022) 81-87 https://doi.org/10.21741/9781644901755-15

Surface Morphology Investigations of Nanocrystalline $R_2Fe_{14}B$ (R = Y, Nd, Gd, Er) by Atomic Force Microscopy

Ivan Pelevin[1,a*], Dmitriy Ozherelkov[1,b], Tatiana Kaminskaya[2,c] and Irina Tereshina[2,d]

[1] Catalysis Lab, National University of Science and Technology MISIS, Moscow, Russia

[2] Faculty of Physics, Lomonosov Moscow State University, Moscow 119991, Russia

[a]i.pelevin@misis.ru, [b] d.ozherelkov@gmail.com, [c]ktp53@mail.ru, [d]irina_tereshina@mail.ru

Keywords: Atomic Force Microscopy, Hard Magnetic Materials, Nanostructured Materials, Rapid Quenching, Melt Spinning, Additive Manufacturing

Abstract. The study was aimed at microstructure investigations of melt-spun rare-earth intermetallic compounds using atomic force microscopy. Surface morphology of $R_2Fe_{14}B$ (R = Y, Nd, Gd, Er) was studied with nanometric resolution. Grain structure features were discovered depending on the rare-earth element composition and quenching regime. Grain size dependence on rare earth elements' composition decreased with the metal's serial number and atomic weight. Wherein structural size dependence on quenching wheel speed had non-linear character: increase the speed from 20 to 30 m/s led to 3 times decrease of the grain size and significant surface roughness reduction.

Introduction

Usually, modern hard magnetic materials are multi-component systems with hysteresis properties provided by precise composition selection and formation of their proper microstructure [1–3]. That is why identifying the relationship between magnetic properties and microstructure continues to be relevant and of great scientific importance applying to both known $R_2Fe_{14}B$ materials (where R – rare earth metal (REM)) and multicomponent alloys $(R,R')_2(Fe,T)_{14}B$ (T = Co, Mn and other) with partial substitution in REM and iron sublattices. The rapid development of synthesis technologies for new nanocrystalline materials requires new analysis methods. There are various synthesis techniques such as powder metallurgy, mechanical synthesis, rapid quenching, severe plastic deformation, and their combinations [4]. Synthesis of permanent magnets by 3D-printing arised recently involving different methods of additive manufacturing. This filed may be divided into two main branches: creating bonded magnets [5–8] and selective laser sintering/melting (SLS/SLM technologies) of powders layer by layer [9–12]. Both approaches could be combined with other technologies such as grain boundary infiltration [10,11,13]. The application of modern additive technologies opens new prospects for permanent magnet manufacturing without any shape limitations. In this regard, SLS/SLM technology is one of the most promising; however, there are still many challenges. In particular, the SLM process assumes specific morphology of the sample surface, which may significantly differ from the internal one [14–17]. Microstructure variation with depth arises due to different cooling conditions and temperature gradients and depends on laser scanning strategy, which usually involves special processing of the layer contour. All described features affect crystallization behavior and thus final grain structure. SLM process assumes high cooling rates of the melting pool (~10^4-10^6 K/s) and thus rapid solidification resulting in superfine microstructure [18–20]. Another conventional rapid solidification technique

providing superfine microstructure applying to Nd-Fe-B-type material is melt-spinning [21–23]. Such technique is rather more used than SLM for now.

It should be noted that all new methods of nanomaterials synthesis require the development of precise structure analysis methods and approaches. The most common metallic materials microstructure characterization method is scanning electron microscopy (SEM), distinguished by relatively easy sample preparation. Transmission electron microscopy (TEM) is usually involved for nano-sized objects observation, but this analytical method requires complicated and thorough sample preparation that limits its usage. Another method of structural (mostly surface) research is atomic force microscopy (AFM). Key advantages of AFM are the possibility of analysis on air or in a liquid medium and the absence of strict requirements for samples (their electrical conductivity, composition, size, magnetic properties).

Previously, the authors carried out a study of multi-component alloys $(Nd,Ho)_2(Fe,Co)_{14}B$ using AFM, which revealed the main features of the microstructure and morphology of their surface in different structural states [24]. The melt-spun samples were obtained, and a study of the topography of their contact and free surfaces was carried out. On the contact side, micron-scale cracks were observed oriented in one preferential direction. The width and depth of the cracks varied from hundreds of nanometers to a few micrometers. The morphology of nano-sized grains and clusters, their size distribution, and homogeneity were determined. The study of the magnetic properties of this material made it possible to establish their relationship with microstructural features.

In studies performed by Jakubowicz [25, 26] $Nd_2Fe_{14}B$/α-Fe-type nanocomposites were investigated using atomic force microscopy. The grain size of samples with various compositions was estimated, and AFM identified their differences. High resolution of the AFM method allowed to discern nanocrystalline grains with an average size of ~19 nm. Besides, small grains tended to form agglomerates with a size of ~250 nm. Height and deflection imaging modes of AFM were used for structural investigations.

Present research work is devoted to investigating the effect of the melt-spinning method on the microstructure of $R_2Fe_{14}B$ alloys with various REM (R = Y, Nd, Gd, Er) using AFM. A comparative study of the variation in the composition of $R_2Fe_{14}B$ alloys (light (Nd) and heavy (Gd, Er) REMs, as well as magnetic (Nd,Gd, Er) rare-earth ions and their nonmagnetic analog (Y) on surface morphology was investigated.

These studies aim to develop a technique for studying the microstructure and surface morphology of melt-spun nanocrystalline magnetic materials based on REMs.. Subsequently, the scope of application of this technique can be extended to similar materials obtained using additive technologies, namely, by the method of selective laser sintering or melting.

Materials and methods

Bulk $Nd_2Fe_{14}B$, $Gd_2Fe_{14}B$, $Er_2Fe_{14}B$ and $Y_2Fe_{14}B$ intermetallic samples were obtained using induction furnace followed by remelting in quartz ampoule and melt supply to the quenching wheel surface (melt spinning technique). Speed of the quenching wheel surface was 20 and 30 m/s. Ribbon-like samples with 10 mm length, 2-5 mm width and ~0.3 mm thickness were obtained. Elemental and phase composition were controlled by means of X-ray fluorescence spectrometry and X-ray diffraction using REAN spectrometer and Difrey-401K (both by "Nauchnie pribory", Russia), respectively. Surface morphology was investigated by atomic force microscopy using an Solver P-47H (NT-MDT, Russia) at room temperature using standard HA_NC Etalon silicon probes (cantilevers) with 94 and 124 μm length and 140-235 kHz frequency range. Obtained data

were processed in Nova RC1 software package. The magnetic hysteresis loops were measured on a standard SQUID magnetometer in fields up to 10 kOe at a temperature of 300 K.

Results and discussions

The analysis of the sample's grain structure was carried out by the AFM method on the initial rapidly quenched samples without any special preparation. This initial state may have a significant effect on the surface morphology and complicate the analysis. Investigation of $Nd_2Fe_{14}B$, $Gd_2Fe_{14}B$, $Er_2Fe_{14}B$ samples was carried out in semi-contact method and in tapping mode using resonance properties of the cantilever.

The structural elements of the surface revealed by this method were considered as grains. The grain size was defined as the diameter of a circle equal to the cross-sectional area of the grain. The average grain size was determined as the square root of the cross-sectional area of the particle at a height corresponding to a given value (0.8). The ratio of the maximum grain section length to the maximum width gives the aspect ratio.

Investigations and comparative analysis of the obtained contact surface structure in the case of samples with a quenching rate of 20 m/s using AFM revealed that the largest average grain size among the investigated intermetallic compounds was for the $Nd_2Fe_{14}B$ compound (see Figure 1a).

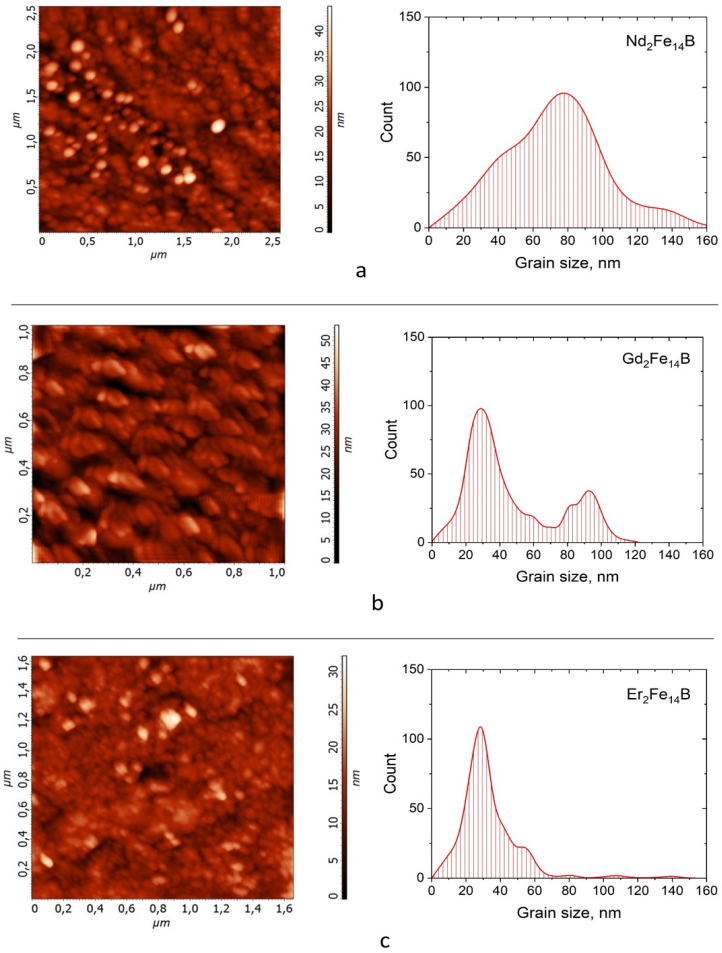

Fig. 1. *AFM images of the contact surface of melt-spun samples obtained at 20 m/s quenching wheel speed (left) and their grain size distributions (right): a – $Nd_2Fe_{14}B$, b – $Gd_2Fe_{14}B$, c – $Er_2Fe_{14}B$.*

The sample structure consisted of regular round shape grains with an average grain diameter of about 70 nm. Additionally, smaller grains with sizes of 30-40 nm were obtained. Partial agglomeration of small grains was observed, giving the total size of structural components up to 150 nm. The contact surface structure of the rapidly quenched $Gd_2Fe_{14}B$ compound was significantly different - see Figure 1b. Grains of $Gd_2Fe_{14}B$ had a highly elongated elliptical shape with dimensions of 30-35 × 90 nm, i.e. aspect ratio of 1:3. The grains' long axis is predominantly oriented along the movement direction of the quenching wheel surface. All grains were collected in agglomerates (bunches), combining around 8-12 grains each and the sizes of agglomerates vary from 120 to 300 nm. The finest grain structure was observed for the $Er_2Fe_{14}B$ melt-spun sample, where grains had a slightly elongated shape with an aspect ratio close to unity. Most grains have a round shape, and the average grain size of 25-30 nm was observed.

Also, some agglomerations up to 100 nm in size were detected. The observed difference in obtained microstructures of melt-spun samples can be explained by the different melting temperatures of the investigated compounds. Different kinetics during quenching, i.e., different temperature gradients, leads to differences in cooling rate and crystallization speed. It is known [27] that crystallization of $Nd_2Fe_{14}B$-type material during rapid quenching proceeds in two stages: at first, $TbCu_7$-type metastable phase arises along with a small amount of α-Fe phase. Then decomposition of the $TbCu_7$-type phase occurs with $Nd_2Fe_{14}B$-type and α-Fe phases formation. Such a two-stage crystallization process complicates the analysis of its kinetics. However, it can be assumed that different rare earth metals that vary from light (Nd) and heavy (Gd and Er) demonstrate different nucleation behavior due to differences in atom radius, weight, and crystal lattice parameters.

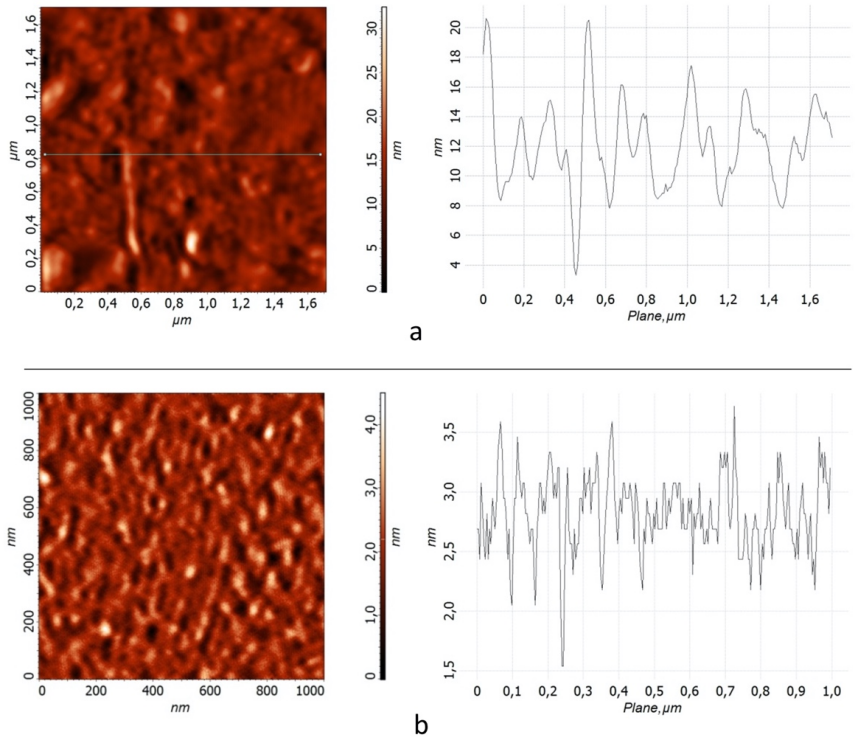

Fig. 2. *AFM images of surface topography (left) of melt-spun $Y_2Fe_{14}B$ obtained at 20 (a) and 30 (b) m/s quenching wheel speeds and profile of their surfaces (right).*

It should be noted that such behavior provides observed nano-sized structure with grain size lower than critical single-domain size. Potentially, it could create optimal conditions for high magnetic properties due to strong exchange coupling between $Nd_2Fe_{14}B$-type and α-Fe phases. Moreover, described crystallization behavior could be expected during synthesis by the novel SLM method, which is planned to attract further research.

Comparative studies of the surface topology of melt-spun $Y_2Fe_{14}B$ samples were carried out with quenching wheel speeds of 20 m/s and 30 m/s. The effect of various quenching speeds is visible in Figure 2. The studies were carried out in a contact mode using the lateral force method. In the contact mode at a distance of a few tenths of a nanometer from the tip of the probe to the sample surface, repulsive forces prevailed. The used method allowed to construct a picture of lateral forces (friction forces) by recording the torsion angle of the probe during scanning in contact with the surface. Moreover, the lateral twisting of the probe was registered simultaneously with topography. In this case, features of the surface relief, which are not resolved in other modes, are visualized due to the different frictional characteristics of the surface. The surface of the sample obtained at a higher speed of 30 m/s is much smoother, and the size of its structural inhomogeneities (i.e., grains) is much smaller. For the 20 m/s sample, the average surface roughness is around 8 nm, and the maximum deviation is 18 nm. The size of structural elements (grains) varied from 70 to 150 nm with agglomerates up to 200 nm. In the case of a 30 m/s sample, the average surface roughness was 1.5 nm, and the maximum emissions were up to 2.5 nm. The size of structural elements (grains) varied from 20 to 50 nm, about 3 times smaller than in the 20 m/s sample. Thus 1.5 times increasing of quenching wheel speed reduced structural element size by 3 times. Such obtained behavior was due to the increased heat dissipation at higher quenching wheel speeds.

Conclusions

The conducted study revealed the structural features of the melt-spun $R_2Fe_{14}B$ samples with various rare earth metals and quenching speeds. The shape and size of the structural elements (grains) were defined by the AFM method. The obtained dependence on rare earth elements in composition demonstrated a decrease of the grain size with the increasing number and atomic weight of the metal. $Nd_2Fe_{14}B$ compound with the lightest rare-earth metal possessed the largest grains among investigated samples. Wherein $Er_2Fe_{14}B$ compound with the heavy rare earth element, on the contrary, quenched with the finest microstructure. An increase of the quenching wheel speed for the $Y_2Fe_{14}B$ compound from 20 to 30 m/s resulted in a significant reduction in surface roughness. Furthermore, the grain size decreased by about 3 times compared to lower quenching speed. Thus, the atomic force microscopy application to nanostructured intermetallic $R_2Fe_{14}B$-type compounds was proposed and worked out with the prospect of using this method for additively manufactured magnetic materials.

Acknowledgments

The work was financially supported by the Russian Science Foundation (RSF), grant › 21-79-10239.

References

[1] J. Mohapatra, J.P. Liu, Rare-Earth-Free Permanent Magnets: The Past and Future, in: Handb. Magn. Mater., 2018: pp. 1–57. https://doi.org/10.1016/bs.hmm.2018.08.001

[2] D. Li, Y. Li, D. Pan, Z. Zhang, C.J. Choi, Prospect and status of iron-based rare-earth-free permanent magnetic materials, J. Magn. Magn. Mater. (2019). https://doi.org/10.1016/j.jmmm.2018.09.032

[3] O. Gutfleisch, M.A. Willard, E. Brück, C.H. Chen, S.G. Sankar, J.P. Liu, Magnetic Materials and Devices for the 21st Century: Stronger, Lighter, and More Energy Efficient, Adv. Mater. 23 (2011) 821–842. https://doi.org/10.1002/adma.201002180

[4] I.S. Tereshina, I.A. Pelevin, E.A. Tereshina, G.S. Burkhanov, K. Rogacki, M. Miller, N. V. Kudrevatykh, P.E. Markin, A.S. Volegov, R.M. Grechishkin, S. V. Dobatkin, L. Schultz, Magnetic hysteresis properties of nanocrystalline (Nd,Ho)-(Fe,Co)-B alloy after melt spinning, severe plastic deformation and subsequent heat treatment, J. Alloys Compd. (2016). https://doi.org/10.1016/j.jallcom.2016.04.228

[5] I.C. Nlebedim, H. Ucar, C.B. Hatter, R.W. McCallum, S.K. McCall, M.J. Kramer, M.P. Paranthaman, Studies on in situ magnetic alignment of bonded anisotropic Nd-Fe-B alloy powders, J. Magn. Magn. Mater. (2017). https://doi.org/10.1016/j.jmmm.2016.08.090

[6] B.M. Ma, J.W. Herchenroeder, B. Smith, M. Suda, D. Brown, Z. Chen, Recent development in bonded NdFeB magnets, J. Magn. Magn. Mater. (2002). https://doi.org/10.1016/S0304-8853(01)00609-6

[7] K. Mungale, T.N. Lamichhane, H. Wang, B.C. Sales, M.P. Paranthaman, U.K. Vaidya, Compression molding of anisotropic NdFeB bonded magnets in a polycarbonate matrix, Materialia. (2021). https://doi.org/10.1016/j.mtla.2021.101167

[8] B.G. Compton, J.W. Kemp, T. V. Novikov, R.C. Pack, C.I. Nlebedim, C.E. Duty, O. Rios, M.P. Paranthaman, Direct-write 3D printing of NdFeB bonded magnets, Mater. Manuf. Process. (2018). https://doi.org/10.1080/10426914.2016.1221097

[9] F. Bittner, J. Thielsch, W.G. Drossel, Laser powder bed fusion of Nd–Fe–B permanent magnets, Prog. Addit. Manuf. (2020). https://doi.org/10.1007/s40964-020-00117-7

[10] C. Huber, H. Sepehri-Amin, M. Goertler, M. Groenefeld, I. Teliban, K. Hono, D. Suess, Coercivity enhancement of selective laser sintered NdFeB magnets by grain boundary infiltration, Acta Mater. (2019). https://doi.org/10.1016/j.actamat.2019.04.037

[11] A.S. Volegov, S. V. Andreev, N. V. Selezneva, I.A. Ryzhikhin, N. V. Kudrevatykh, L. Mädler, I. V. Okulov, Additive manufacturing of heavy rare earth free high-coercivity permanent magnets, Acta Mater. (2020). https://doi.org/10.1016/j.actamat.2020.02.058

[12] F. Bittner, J. Thielsch, W.G. Drossel, Microstructure and magnetic properties of Nd-Fe-B permanent magnets produced by laser powder bed fusion, Scr. Mater. (2021). https://doi.org/10.1016/j.scriptamat.2021.113921

[13] L. Li, A. Tirado, B.S. Conner, M. Chi, A.M. Elliott, O. Rios, H. Zhou, M.P. Paranthaman, A novel method combining additive manufacturing and alloy infiltration for NdFeB bonded magnet fabrication, J. Magn. Magn. Mater. (2017). https://doi.org/10.1016/j.jmmm.2017.04.066

[14] I. Yadroitsev, I. Smurov, Surface morphology in selective laser melting of metal powders, in: Phys. Procedia, 2011. https://doi.org/10.1016/j.phpro.2011.03.034

[15] G. Strano, L. Hao, R.M. Everson, K.E. Evans, Surface roughness analysis, modelling and prediction in selective laser melting, J. Mater. Process. Technol. (2013). https://doi.org/10.1016/j.jmatprotec.2012.11.011

[16] S. Gao, X. Yan, C. Chang, Eric Aubry, M. Liu, H. Liao, N. Fenineche, Effect of Laser Energy Density on Surface Morphology, Microstructure, and Magnetic Properties of Selective Laser Melted Fe-3wt.% Si Alloys, J. Mater. Eng. Perform. (2021).

https://doi.org/10.1007/s11665-021-05591-w

[17] M. Zheng, L. Wei, J. Chen, Q. Zhang, J. Li, S. Sui, G. Wang, W. Huang, Surface morphology evolution during pulsed selective laser melting: Numerical and experimental investigations, Appl. Surf. Sci. (2019). https://doi.org/10.1016/j.apsusc.2019.143649

[18] P.A. Hooper, Melt pool temperature and cooling rates in laser powder bed fusion, Addit. Manuf. (2018). https://doi.org/10.1016/j.addma.2018.05.032

[19] Y. Li, D. Gu, Parametric analysis of thermal behavior during selective laser melting additive manufacturing of aluminum alloy powder, Mater. Des. 63 (2014) 856–867. https://doi.org/10.1016/j.matdes.2014.07.006

[20] M. Majeed, H.M. Khan, I. Rasheed, Finite element analysis of melt pool thermal characteristics with passing laser in SLM process, Optik (Stuttg). (2019). https://doi.org/10.1016/j.ijleo.2019.163068

[21] J.J. Croat, Manufacture of NdFeB permanent magnets by rapid solidification, J. Less-Common Met. (1989). https://doi.org/10.1016/0022-5088(89)90006-4

[22] A. Zaluzka, Y. Xu, Z. Altounian, J.O. Strom-Olsen, Effects of quench rate on the texture in melt-spun NdFeB alloys, Mater. Sci. Eng. A. (1991). https://doi.org/10.1016/0921-5093(91)90193-Q

[23] H.C. Hua, G.Y. Wang, C.H. Zheng, G.X. Huang, Q.Z. Xu, L.H. Wu, S.Y. Shi, Microstructure of melt-spun NdFeB magnet, Mater. Lett. (1988). https://doi.org/10.1016/0167-577X(88)90085-7

[24] N. V. Andreeva, A. V. Filimonov, A.I. Rudskoi, G.S. Burkhanov, I.S. Tereshina, G.A. Politova, I.A. Pelevin, A study of nanostructure magnetosolid Nd–Ho–Fe–Co–B materials via atomic force microscopy and magnetic force microscopy, Phys. Solid State. (2016). https://doi.org/10.1134/S1063783416090079

[25] J. Jakubowicz, Application of atomic force microscopy in microstructure analysis of mechanically alloyed Nd2Fe14B/α-Fe-type nanocomposites, J. Alloys Compd. (2003). https://doi.org/10.1016/S0925-8388(02)01075-7

[26] J. Jakubowicz, Application of AFM to study functional nanomaterials prepared by mechanical alloying, in: J. Mater. Sci., 2004. https://doi.org/10.1023/B:JMSC.0000039249.21167.a5

[27] K. Men, K. Li, Y. Luo, D. Yu, K. Zhang, J. Jin, Y. Mao, The crystallization behavior of as-quenched Nd9Fe85Nb0.5B5.5 alloys, J. Alloys Compd. (2015). https://doi.org/10.1016/j.jallcom.2015.02.046